Two-Dimensional Infrared Spectroscopy of the Alanine Dipeptide in Aqueous Solution

Yung Sam Kim, Jianping Wang, and Robin M. Hochstrasser*

Department of Chemistry, University of Pennsylvania, Philadelphia, Pennsylvania 19104-6323

Received: November 2, 2004; In Final Form: December 17, 2004

The linear-infrared and two-dimensional infrared (2D IR) spectra in the amide-I′ region of the alanine dipeptide and its ^{13}C isotopomers in aqueous solution (D_2O) are reported. The two amide-I′ IR transitions have been assigned unambiguously by using ^{13}C isotopic substitution of the carbonyl group; the amide unit at the acetyl end shows a lower transition frequency in the unlabeled species. The ratio of their transition dipole strengths remains almost unchanged upon ^{13}C substitution, indicating the absence of intensity transfer between two vibrators. The 2D IR cross peaks directly associated with intramode coupling in this case show a small off-diagonal anharmonicity (0.2 ± 0.2 cm^{-1}), leading to a small coupling constant (1.5 ± 0.5 cm^{-1}). The coupling and the 2D IR spectra in two different polarizations ($\langle zzzz \rangle$ and $\langle zxxz \rangle$) are as expected for a polyproline-II (PP_{II})-like conformation for dialanine, with the backbone dihedral angles (ϕ, ψ) determined to be in the range of ($-70° \pm 25°$, $+120° \pm 25°$). Ab initio DFT calculations and normal mode decoupling analysis in the Ramachandran subspace in the neighborhood of PP_{II} conformation confirm the presence of a region where the coupling is vanishingly small and support these experimental findings. The relationship between the coupling and off-diagonal anharmonicity is consolidated by examining the distribution of the latter from an ensemble averaged Hamiltonian incorporating uncorrelated diagonal frequency distributions and a small coupling (<2 cm^{-1}); it is found that the most probable value for the off-diagonal anharmonicity falls into the range of experimental observations. Further, incorporating DFT results, the simulated linear-IR and 2D IR can reproduce the essential features of the measurements, including the transition frequency positions and apparent peak intensities. All the experimental results and simulations are consistent with a PP_{II}-like conformation for the alanine dipeptide in aqueous solution, in which two amide-I′ modes are highly localized and whose frequency distributions are uncorrelated.

1. Introduction

For the past two decades there have been many experimental and theoretical studies on the conformations of dipeptides in various solvents,[1−7] particularly in water. Dipeptides, the basic building units of proteins, have been used as model systems to test predictions of the secondary structures adopted by solvated peptides. The alanine dipeptide in water is one of these model systems that has been frequently considered in the past. Several configurations of the alanine dipeptide, such as the polyproline-II (PP_{II}), the right-handed α-helix (α_R), and the internal hydrogen-bonded (C_5 and C_7) structures, have been suggested as stable ones depending on whether there exists an internal hydrogen bond or an external hydrogen bond to the solvent. In general, it is believed that the solvent polarity determines the hydrogen bonding character of the peptide. Despite many studies, there is not agreement on the solvated structures of the alanine dipeptide. For example, CD and NMR techniques[1] and ^{13}C NMR[4] indicate that PP_{II} and α_R structures coexist in water, while density functional theory (DFT),[3] and other NMR experiments[7] suggest that the PP_{II} structure is the dominant one and only a slight amount of the α_R structure is to be found in aqueous solutions. Studies using CHARMM[8] molecular dynamics simulations[5] predicted the α_R structure is the dominant one in water. A recent study by means of Raman spectroscopy[6] suggested that the C_{7eq} structure is enthalpically the most stable one in water. Clearly there is a need for further experimental examination of this basic element of peptide structure.

Recent experimental[9−11] and theoretical[12] developments in multidimensional infrared spectroscopies, 2D IR and 3D IR, have made it possible to obtain structural features and equilibrium dynamics of peptides and proteins by means of pump−probe techniques and time and spectral domain interferometry.[13−18] The cross peaks appearing in the 2D IR spectra indicate whether the excitation of one mode influences the frequency of the others and hence the extent to which modes are coupled. Also 2D IR experiments in polarized light can measure the angles between the dipoles of the IR transitions which can yield in turn the relative orientation of the two amide planes that are involved in the transitions during the four-wave mixing processes. The extension to 3D IR records these 2D IR echo signals along a waiting time axis (T) in order to provide information on the decay of the frequency correlations of the vibrators in analogy with stimulated photon echo experiments on electronic transitions.[19]

In this paper we present a study of the alanine dipeptide in D_2O using multidimensional infrared spectroscopies. In the experiments two different ^{13}C labelings of the dipeptide were employed in order to spectrally separate the otherwise overlapping two amide modes. By substituting $^{12}C{=}^{16}O$ with $^{13}C{=}^{16}O$ in an amide group we lower the transition frequency of the amide-I′ mode by ca. 40 cm^{-1}.[18] The present work aims to establish features of the structures of the alanine dipeptide in water.

* Corresponding author. Tel: 215-898-8203; Fax: 215-898-0590; E-mail: hochstra@sas.upenn.edu

10.1021/jp044989d CCC: $30.25
Published on Web 03/19/2005

2. Materials and Methods

The multidimensional IR spectra were obtained using heterodyned spectral domain interferometry using the basic laser arrangement described in detail previously.[10,14,18] Three 300 nJ infrared pulses with wave vectors k_1, k_2, and k_3 were incident on the sample. The sequence of the three pulses was varied and we refer to the interval between pulse 1 and 2 as τ, between 2 and 3 as T, and between 3 and the detected signal as t. For example, k_1 arrives earlier than k_2 by an amount τ in the rephasing scheme, while k_2 arrives earlier than k_1 in the nonrephasing scheme. In both cases k_3 is the last pulse to arrive at the sample. The phase-matched signal at wave vector $-k_1+k_2+k_3$ is detected as a function of the time intervals. The local oscillator pulse always preceded the signal pulse by ~1.5 ps. The spatially overlapped signal and local oscillator pulses were dispersed in a monochromator having a 64-element MCT array detector (IR Associates, Inc.) at its focal plane. Each detector element is 200 μm in width and 1 mm in height. The focal length of the monochromator is 270 mm and the groove density of the grating used in our experiments was 120 lines/mm. The raw data collected using this method were in the form of a two-dimensional array of time, in 2 fs steps, and wavelength, in ~6 nm steps. For example in the rephasing case, the columns and rows of the array are the time delays τ and wavelengths, respectively. The raw data is in the form of $\tilde{S}(\tau,T,\lambda_k)$. By performing an inverse Fourier transform to the time domain followed by a Fourier transform to the frequency domain we converted $\tilde{S}(\tau,T,\lambda_k)$ into $\tilde{S}(\tau,T,\omega_m)$, where λ_k represents corresponding wavelength of the kth (k = 1...64) detector element and ω_m represents mth of 400 evenly spaced frequencies. The two Fourier transforms were performed as follows. The inverse Fourier transform was

$$S(\tau,T,t) = \sum_{k=1}^{64} \tilde{S}(\tau,T,\lambda_k) \exp(i\omega_k t)\, \Delta\omega_k$$
$$t = 0,1,2,...,5000 \text{ fs} \qquad (1)$$

where $\omega_k = 2\pi c/\lambda_k = 2\pi c/(\Delta\lambda(k-32) + \lambda_{32})$ and $\Delta\omega_k = 2\pi c/(\Delta\lambda(k-32-1/2)+\lambda_{32}) - 2\pi c/(\Delta\lambda(k-32+1/2)+\lambda_{32})$. $\Delta\lambda$ is the wavelength difference between two adjacent detector elements and is a constant in a limited spectral range. λ_{32} is the wavelength observed by the 32nd element of the detector. The $S(\tau,T,t)$ was Fourier transformed to generate $\tilde{S}(\tau,T,\omega_m)$.

$$\tilde{S}(\tau,T,\omega_m) = \sum_m S(\tau,T,t) \exp(-i\omega_m t)\, \Delta t \qquad (2)$$

At this point $\tilde{S}(\tau,T,\omega_m)$ is in the form of $\tilde{S}(\tau,T,\omega_t)$. The spectra were obtained as combined frequency time data sets defined as $\tilde{S}_R(\tau,T,\omega_t)$ and $\tilde{S}_{NR}(\tau,T,\omega_t)$ where R and NR refer to the rephasing and non-rephasing configurations. Using procedures described by Joffre and co-workers,[20,21] the processed signals $\tilde{S}_R(\tau,T,\omega_t)$ and $\tilde{S}_{NR}(\tau,T,\omega_t)$ were obtained by Fourier transformation of the $\tilde{S}$ signals along ω_t followed by back Fourier transformation of only the positive frequency component. The complex 2D IR spectra $\underline{S}_R(-\omega_\tau,T,\omega_t)$ and $\underline{S}_{NR}(\omega_\tau,T,\omega_t)$were then obtained by Fourier transformation along τ. In the experiments, the center frequency of the pulses was ~1620 cm^{-1}, which was chosen to be near the intensity median of the amide-I′ absorption region spectrum being examined. For 2D IR, data sets were collected at two different grating positions, one centered at 1590 cm^{-1} and the other at 1660 cm^{-1}. For pump-probe experiments we combined data from four different grating positions. The waiting time dependent spectra were obtained at 26 values of T ranging from 0 to 2 ps.

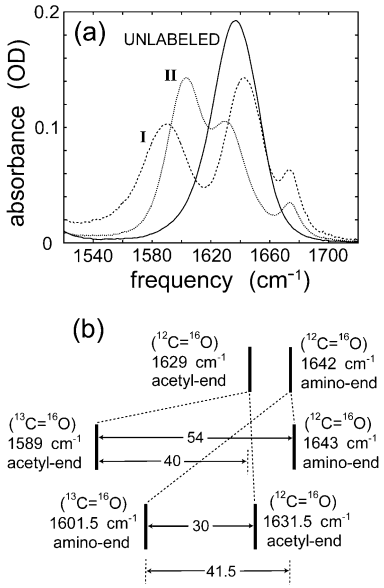

Figure 1. (a) Linear FTIR spectra of the alanine dipeptide isotopomers in D_2O: the unlabeled, isotopomer I ($^{13}C{=}^{16}O$ labeled on the acetyl end) and isotopomer II ($^{13}C{=}^{16}O$ labeled on the amide end). (b) Schematic diagram representing center frequencies of the transitions for three isotopomers.

Samples. The two isotopically labeled alanine dipeptide samples were purchased from Synpep Corporation and the isotopically unlabeled alanine dipeptide sample was purchased from Bachem. They were used without further purification. The compound labeled by $^{13}C{=}^{16}O$ on the acetyl end is referred to as the isotopomer I while the one labeled on the amino end is the isotopomer II. The concentrations of the samples were ~70 mM in D_2O, and the optical densities of the samples for the amino end peak were ~0.14 OD using a 25 μm path length. The cell material was CaF_2. The sample contained some trifluoroacetic acid (TFA) as impurity. Based on our measurements, the mole fractions of TFA molecules in isotopomer I and II were 7% and 5%, respectively, of those of the alanine dipeptide. The extinction coefficient of TFA is $\epsilon_{max} \sim 1800$ cm^{-1} M^{-1}, and that of the alanine dipeptide is $\epsilon_{max} \sim 800$ cm^{-1} M^{-1}.

3. Results and Discussion

FTIR Spectra of the Alanine Dipeptide. The linear-IR spectra of the alanine dipeptide and its isotopomers each show two transitions in the amide-I′ region. The spectra are shown in Figure 1 with the band positions and assignments indicated. The weak band at 1674 cm^{-1} is due to TFA. The peak positions and intensities for the unsubstituted molecule, which shows only one asymmetric absorption band, were obtained by curve fitting the spectrum to two overlapped Voigt profiles. The fit with peaks at 1642 and 1629 cm^{-1} was excellent. The isotopic substitution clearly points to the assignment of these transitions to the acetyl (N-terminal) and amino (C-terminal) ends of the peptide. The experimental transition dipole strengths obtained by integration of the FTIR spectra were quite similar to the value appearing Torii and Tasumi's paper (0.37 D)[22] for an amide-I′ mode. The strengths from our experiments were 0.40 D for the 1642 cm^{-1} and 0.38 D for the 1629 cm^{-1} bands. The 1642 cm^{-1} band undergoes a 40.5 cm^{-1} shift, while the 1629 cm^{-1} band shifts by only 2.5 cm^{-1} when the amino end is isotopically substituted with $^{13}C{=}^{16}O$ (isotopomer II). Isotopic

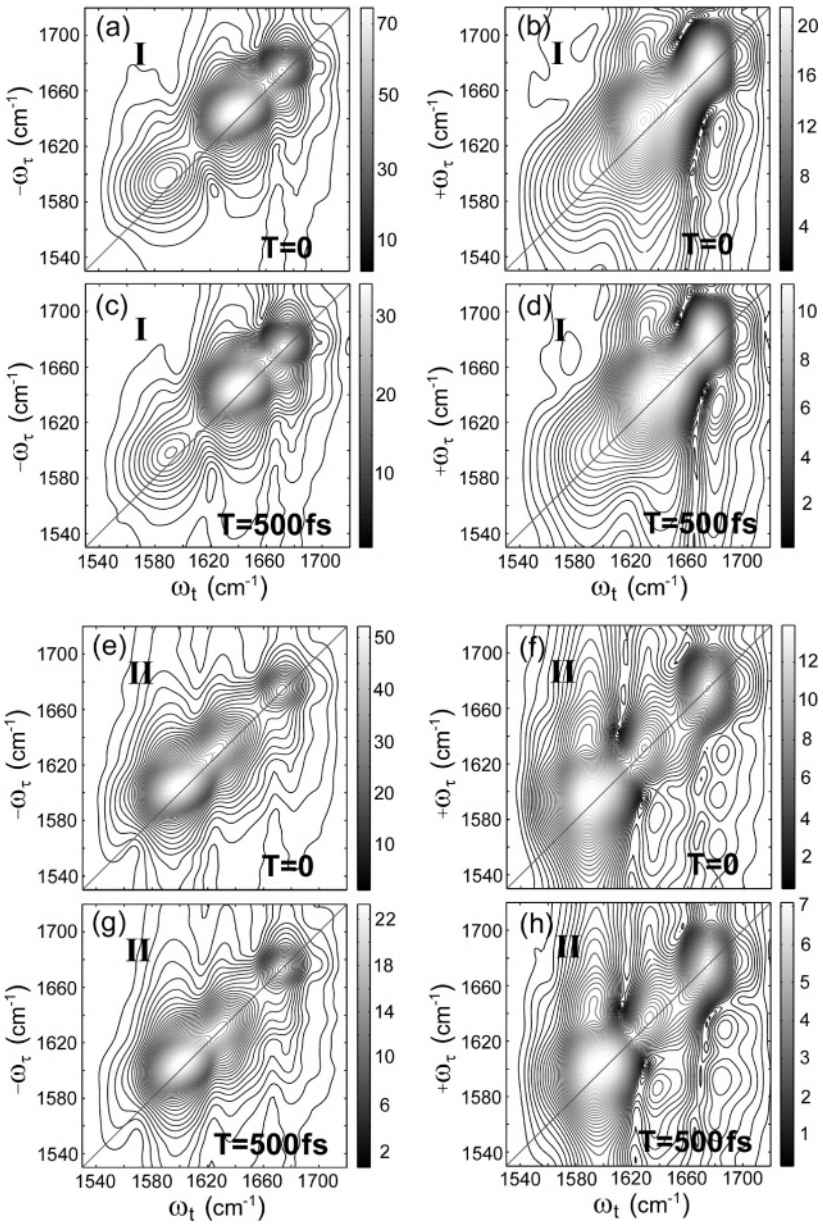

Figure 2. Absolute part of the 2D IR spectra of isotopomer I and isotopomer II, at $T = 0$ and $T = 500$ fs. Left column is for the rephasing and right column for the non-rephasing. Waiting times are given in each plot. (a−d) are for the isotopomer I and (e−h) are for the isotopomer II.

substitution of only the acetyl group (isotopomer I) leads to an isotope shift of 40 cm^{-1} of the 1629 cm^{-1} band, while the 1642 cm^{-1} band is shifted by only 1.0 cm^{-1}. If the splitting of 13 cm^{-1} in the unsubstituted peptide obtained from the fitting was exclusively caused by the coupling between the two amide modes and if the isotope shifts were the same, say 41 cm^{-1}, for the two ends, then the two isotopomers would be expected to have the same peak positions in the FTIR spectra in the amide-I′ region. These spectra would consist of two transitions separated by 42.5 cm^{-1}. Instead, the linear spectra are consistent with two approximately localized modes separated by 13 cm^{-1}, each with about the same isotope shift of 41 ± 1 cm^{-1}. In other words, the unsubstituted form has amide modes that are approximately localized on the ends of the peptide. It is therefore a significant challenge to determine the coupling, which must be very small. Calculations based on a CHARMM force field predicted that the two modes will be nearly localized in the alanine dipeptide,[5] but the frequency ordering of the modes was the opposite of what is observed here. The two ends of the molecule are chemically different, unrelated by symmetry so it is not surprising that they exhibit different vibrational frequencies. The peak intensity ratios of amide-I′ modes of the amino end to acetyl end of the three alanine dipeptides, were 1:0.935, 1:0.905, and 1:0.870 for the unsubstituted compound, isotopomer I, and isotopomer II, respectively. If these small changes in relative intensity were considered to be caused by coupling between the amide-I′ modes, it is straightforward to show from two level quantum mechanics, for example see ref 23, that this coupling would require to be positive and less than a few cm^{-1}. Although the intensity patterns are consistent with such coupling, there is not compelling evidence that the coupling between amide-I′ modes is responsible for these intensity variations.

Multidimensional Infrared Spectra. The principles governing the non-rephasing and rephasing contributions to the 2D IR spectra of coupled oscillators in peptides have been described previously.[24,25] In the ensuing discussion the fundamentals of the acetyl and amino end oscillators are labeled as 1 and 2, their overtones as 1+1 and 2+2 and the combination as 1+2. In the rephasing process the first pulse generates sub-ensembles

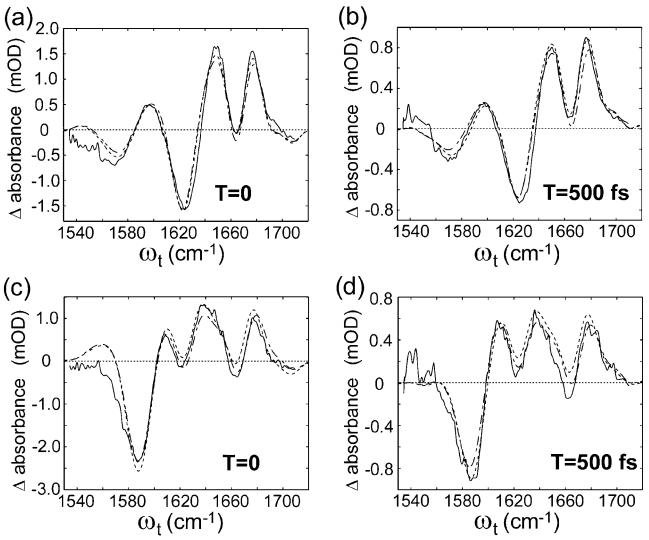

Figure 3. Comparison of pump−probe spectra and projection of 2D IR spectra onto the ω_t axis. Waiting times are given in each plot. (a, b) are for the isotopomer I and (c, d) are for the isotopomer II. Solid line: pump−probe spectra; dashed line: projection of the rephasing spectra; broken dashed line: projection of the non-rephasing spectra.

of molecules having coherences $\rho_{01}^{(1)}$ or $\rho_{02}^{(1)}$, which are allowed to evolve for time period τ. The second pulse creates populations $\rho_{00}^{(2)}$, $\rho_{11}^{(2)}$, and coherence $\rho_{21}^{(2)}$ in the first ensemble and $\rho_{00}^{(2)}$, $\rho_{22}^{(2)}$, and coherence $\rho_{12}^{(2)}$ in the second, which are examined during the waiting time period T. Through allowed IR transitions undergone by the six resulting groups of molecules, the third pulse creates the coherences $\rho_{10}^{(3)}$, $\rho_{20}^{(3)}$, $\rho_{1+1,1}^{(3)}$, $\rho_{1+2,1}^{(3)}$, $\rho_{2+2,2}^{(3)}$, and $\rho_{1+2,2}^{(3)}$, which each contribute to the third-order macroscopic polarization and contribute to the radiated field at their characteristic frequencies, indicated by the subscripts, leading to the spectrum distributed along the ω_t axis. The non-rephasing processes lead to these same six coherences but they arise from the conjugates of the coherences created in the τ period. The dynamics of the frequencies are described by means of the relaxation functions defined by Mukamel.[26] The population relaxation times measured by heterodyned transient grating experiments[27] are introduced into the responses as phenomenological parameters. The 2D IR spectra are composed from a set of peaks on the ω_τ-axis, corresponding in frequency to those seen in the linear spectrum, that become spread out on the ω_t-axis to create peaks at the oscillation frequencies of all the coherences mentioned above. Other processes in the third order response, for example third harmonic generation, are not observed in the phase matched direction and frequency range chosen for the experiment. The results of the 2D IR spectra are presented in various forms to facilitate the interpretation of different features. Generally the spectra consist of diagonal peaks that are the $v = 0 \rightarrow v = 1$ transitions and those shifted along the horizontal axis by the diagonal anharmonicity which are the $v = 1 \rightarrow v = 2$ or combination band transitions of the peptide. It will be seen that the isotope shifts of ca. 40 cm^{-1} ensure that the system of two oscillators is in the weak coupling limit.

The 2D IR Spectra. The absolute magnitudes of the complex spectra $\underline{S}_R(-\omega_\tau,T,\omega_t)$ and $\underline{S}_{NR}(\omega_\tau,T,\omega_t)$ of the alanine dipeptide are shown in Figure 2 for two representative values of the waiting time, $T = 0$ and $T = 500$ fs. The cross peaks are very weak and barely discernable by visual inspection of the 2D IR spectra. Figure 3 shows the broadband pump/broadband probe spectra $P_{exp}(T,\omega_t)$ for both isotopomers at two representative times $T = 0$ and $T = 500$ fs. Also shown in Figure 3 are the projections of the 2D IR spectra, $P_{proj}(T,\omega_t)$, which could be obtained from the R and NR data by two different data analysis procedures. In one approach the projection was defined[28] as

$$P_{proj}(T,\omega_t) = \mathrm{Re}\{\int_{band} d\omega_\tau e^{i\phi}\underline{S}(\omega_\tau,T,\omega_t)\} \qquad (3)$$

where the integral symbolizes a discrete summation over the whole bandwidth of the experimental spectrum, determined as described above, which incorporates a presumed accurately measured value of the time interval between the local oscillator and the signal. The phase angle ϕ was varied until the best correspondence was obtained between $P_{exp}(T,\omega_t)$ and $P_{proj}(T,\omega_t)$. This procedure generated a value of $\phi = \phi_0$ that permitted a 2D IR spectrum to be obtained that we show to represent approximately the real part of the 2D IR spectrum. Within experimental error the same projections were obtained from the rephasing and non-rephasing spectra. In the other approach the time delay between the local oscillator and the signal pulse was adjusted in small fractions of a cycle around the experimentally determined fixed delay until the projection of the real part of the calculated complex spectrum matched most closely the pump−probe spectrum. Again within experimental error the two approaches just described generated the same projections from the data set. In fact the phase shift ϕ_0 was equal to the carrier frequency times the fixed delay. We also made ϕ a function of ω_t in order to incorporate the effects of the frequency variations of the phase difference between the local oscillator and the signal beam caused by calcium fluoride windows. However we found that the spectra obtained with a constant ϕ were not significantly distorted by the differences in the optical paths for the two beams, so this refinement was not incorporated. Therefore what we refer to as real spectra resemble very closely the actual real parts of the complex spectra. The agreement with the pump−probe spectra is within experimental error in all cases.

Correlation 2D IR Spectra. Figure 4 shows the real parts of the rephasing and non-rephasing spectra, $\mathrm{Re}\{e^{i\phi_0}\underline{S}(\mp\omega_\tau,T,\omega_t)\}$, at two representative waiting times. Here the "−" and "+" in "∓" refer to the rephasing and the non-rephasing parts of the spectra. The coupling peaks between the two amides in the molecule are not evident in the spectra of isotopomer I, but for II, for which the frequencies are closer, these real spectra show a very small but definitive coupling peak. The correlation spectra are shown in Figure 5 at the same two representative waiting times. To obtain these spectra we combined $\tilde{S}_R(\tau,T,\omega_t)$ and $\tilde{S}_{NR}(\tau,T,\omega_t)$ along the τ-axis then Fourier transformed the combined data along the τ-axis. The combined data uses $\tilde{S}_{NR}(\tau,T,\omega_t)$ values for negative τ, and $\tilde{S}_R(\tau,T,\omega_t)$ values for positive τ. This way of summing reduces the error caused by spectral phase mismatch of the real rephasing and non-rephasing spectra. These combined spectra are the same as those obtained by adding the real rephasing $\underline{S}_R(-\omega_\tau,T,\omega_t)$ and non-rephasing spectra $\underline{S}_{NR}(\omega_\tau,T,\omega_t)$ at each $|\omega_\tau|$.[29] The individual rephasing and non-rephasing spectra also provide useful clues regarding the existence of underlying peaks in the spectrum.[24,30]

The correlation spectra indicate a number of features. Again the weak cross peaks in isotopomer II are more apparent than are any cross peaks in I. These results compared with other reported measurements of peptide 2D IR indicate that the coupling between the amide groups is relatively weak in the alanine dipeptide. The other obvious feature is that the diagonal anharmonicities of the two amides are about the same. A detailed analysis shows that they are 15.5 and 16.0 cm^{-1} for the amino end and acetyl end, respectively. These values were consistent with those measured from the two quantum signals mentioned below.

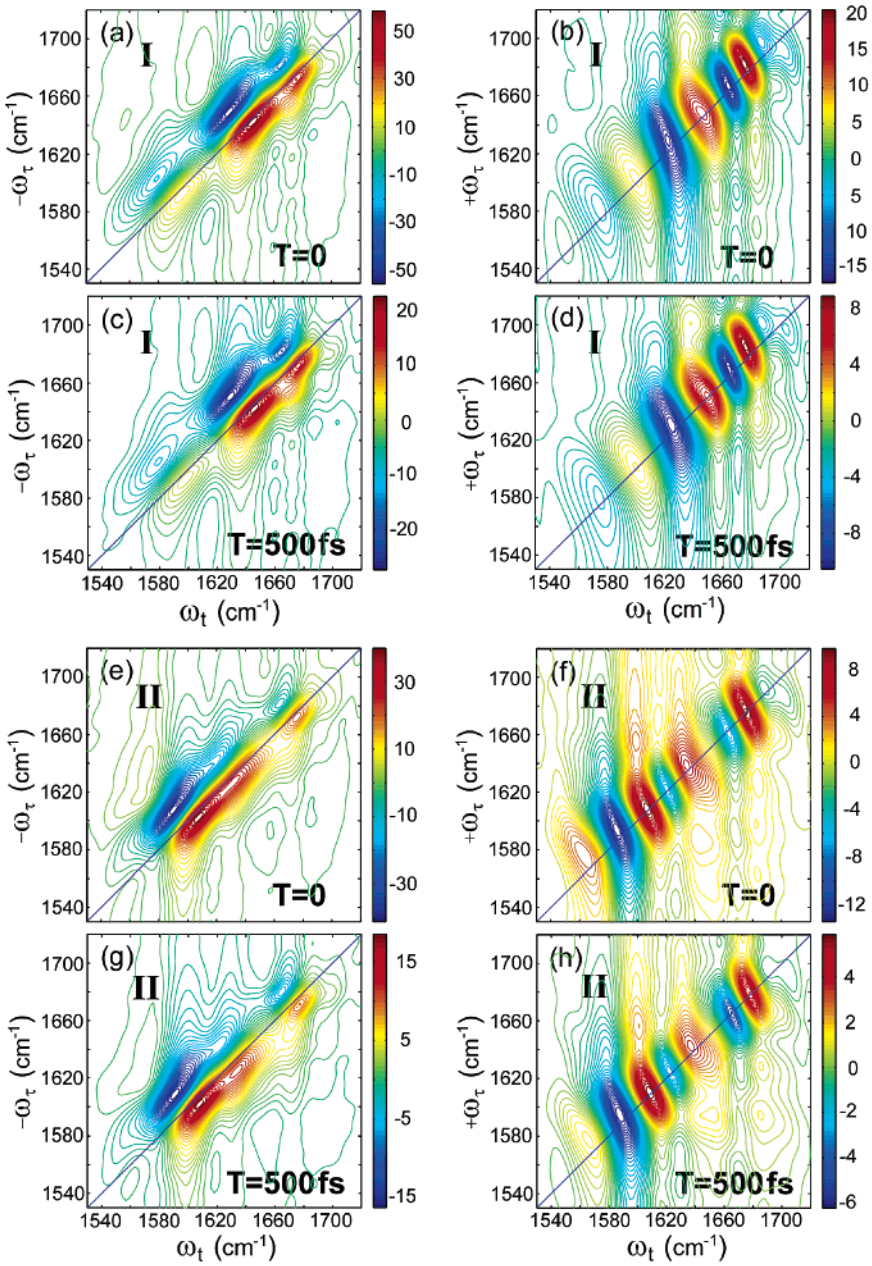

Figure 4. Real part of the 2D IR spectra of isotopomer I and isotopomer II, at $T = 0$ and $T = 500$ fs. Left column is for the rephasing and right column for the non-rephasing. Waiting times are given in each plot. (a−d) are for the isotopomer I and (e−h) are for the isotopomer II.

We have also noted the appearance of a transition around 1560 cm^{-1} in the unsubstituted dialanine (data not shown) and isotopomer II, present at $T = 0$ in 2D IR but not evident in the FTIR spectra. Its intensity is ca. 1−5% of those of the main peaks. This peak can be seen in Figure 5c and it exhibits cross peaks with the alanine amide I′ modes of both the acetyl end and amino ends of the peptide. This transition appear to be associated with the acetyl end which is why it is not observed when the acetyl end is isotopically substituted but is observed with the other two isotopomers. Since the 2D IR spectral signal varies linearly with the product of the optical density and the extinction coefficient of the transition, it is possible to have peaks show up in 2D IR and not in the linear spectrum. We also have observed cross peaks between TFA and alanine dipeptide, which must be due to some molecules of the alanine dipeptide that are bound to TFA.

The population relaxation of the $v = 1$ states of amino and acetyl amides, respectively, for the isotopomer I were measured by means of heterodyne transient grating signals.[27] Each required fitting to two exponentials having time constants, 576 fs (relative amplitude of 74%) and 1850 fs (26%) for the amino amide and 415 fs (86%) and 5700 fs (14%) for the acetyl amide.

Non-rephasing Two Quantum Transitions. Figures 6a−6d report the experiments in which the pair of time coincident pulses at k_3 and k_2 are followed by one at k_1 after a time interval that we continue to label as τ. After the second pulse a fraction of the molecules are in the coherent states $\rho_{1+1,0}$, $\rho_{2+2,0}$, and $\rho_{1+2,0}$. This signal, still in the direction $-k_1+k_2+k_3$, oscillates along the τ-axis at approximately twice the frequency of the amide-I′ mode. Experiments involving such two quantum pulse sequences have been reported recently by Zanni and coworkers.[31] The coherent states with two vibrational quanta decay by the dephasing of the two quantum states and the 2D IR spectra provide their anharmonicities. For example, the relaxation times of two quantum signals initiated by 1602 and 1632 cm^{-1} excitations of the isotopomer II were 174 and 159 fs. They

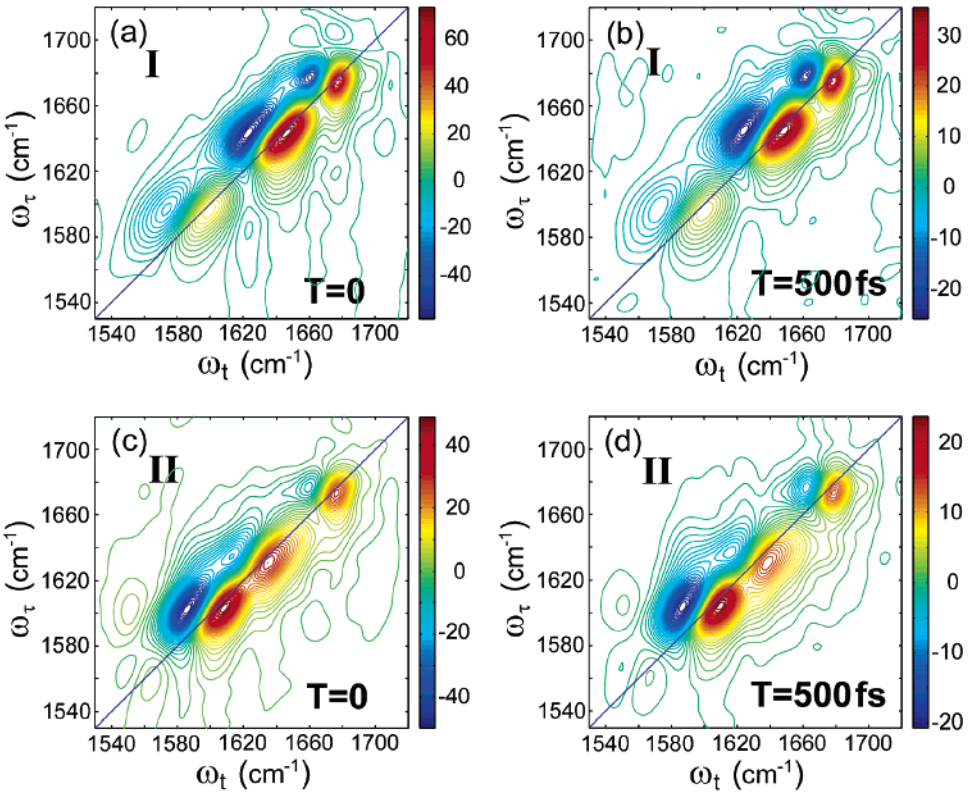

Figure 5. Real part of absorptive 2D IR spectra of the isotopomer I and II. Waiting times are given in each plot. (a, b) are for the isotopomer I and (c, d) are for the isotopomer II.

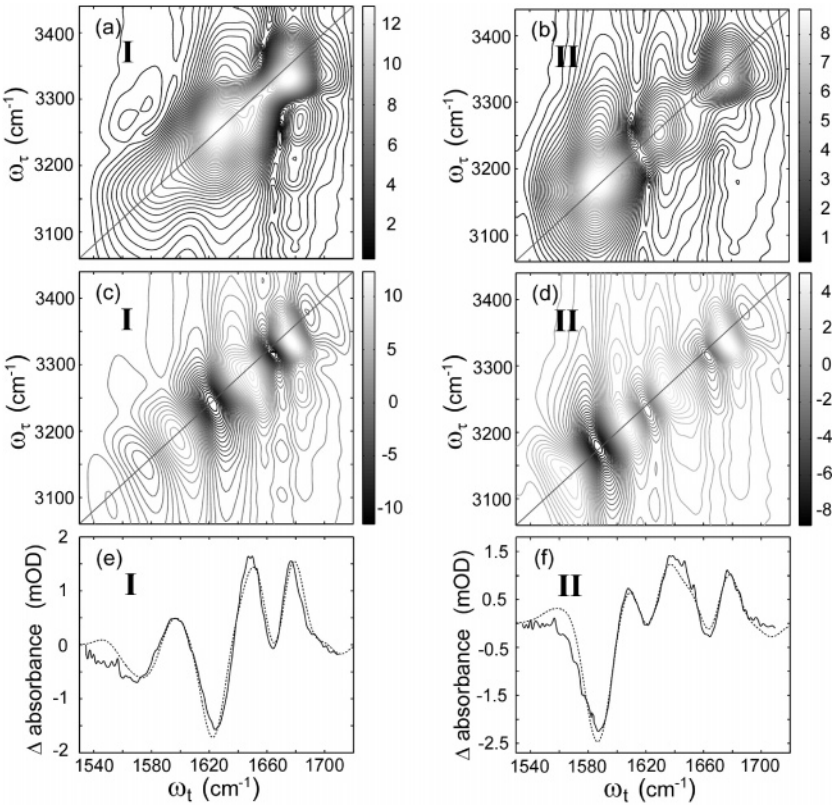

Figure 6. The 2D IR spectra of two quantum states along the ω_τ-axis and one quantum state along the ω_t-axis in comparison with pump−probe spectra. (a, c, e) for the isotopomer I; and (b, d, f) for the isotopomer II. (a, c) are the absolute part of the 2D IR spectra; (c, d) are the real part of the 2D IR spectra; and (e, f) are projections in comparison with the pump−probe. Solid line: pump−probe spectra; dashed line: projection of the 2D IR spectra.

were 320 fs at 1602 cm^{-1} and 282 fs at 1632 cm^{-1} along non-rephasing direction. The spectra in Figure 6 closely resemble the corresponding one quantum non-rephasing spectra that are shown in Figure 4, except for the values of the frequency on

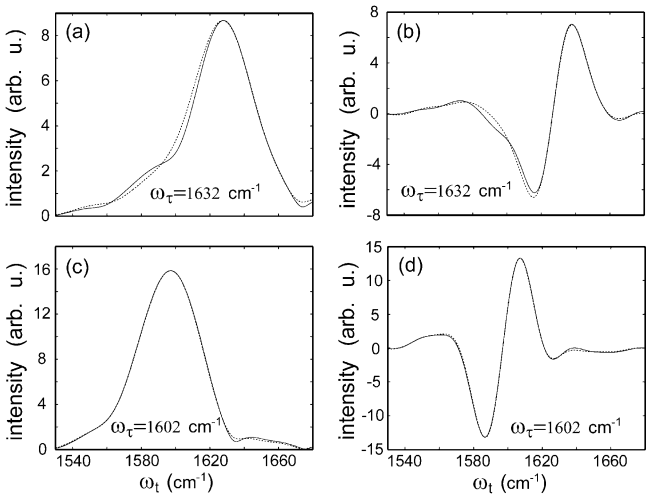

Figure 7. Trace of the real and absolute magnitude parts of the absorptive 2D IR spectra for the isotopomer II at $\omega_\tau = 1602$ cm^{-1} and $\omega_\tau = 1632$ cm^{-1}. (a) The magnitude at $\omega_\tau = 1632$ cm^{-1}. (b) The real part at $\omega_\tau = 1632$ cm^{-1}. (c) The magnitude at $\omega_\tau = 1602$ cm^{-1}. (d) The real part at $\omega_\tau = 1602$ cm^{-1}. Solid line: $\langle zzzz\rangle$; dashed line: $3\langle zxxz\rangle$.

the ω_τ-axis, which are roughly twice those of the corresponding non-rephasing spectra. In Figure 6 the frequencies are $\omega_{k+k,0} = 2\omega_{k0} - \Delta_k$, $k = 1,2$. The anharmonicities obtained from Figure 6 are $\sim$16 cm^{-1} for both of the amide I′ modes of isotopomer II in agreement with the 2D IR echo measurement. The comparison of the pump−probe and the projection of this signal are shown in Figure 6e and 6f. This two quantum signal does not give rise to a conventional echo.

Angular and Coupling Constraints. Near the cross peak region, the experimental curves for the two polarizations are slightly different indicating the presence of underlying cross peaks. The small cross peak contribution is superimposed on the tail of the strong diagonal peaks. Previous works[32,33] have shown that when the transition dipoles of the two amide modes are parallel or antiparallel, the contributions of the cross peak to the signal has the same polarization property as the diagonal regions, which is that the $\langle zzzz\rangle$ signal is three times the $\langle zxzx\rangle$ signal. More generally the $\langle zzzz\rangle$ cross peak signal is proportional to $(4P_2+5)/45$ while that of $\langle zxzx\rangle$ is proportional to $P_2/15$, where P_2 is the average value of the second Legendre polynomial of the cosine of the angle θ between the transition dipoles.[32] When the two dipoles are oriented at the magic angle ($\theta_m = 54.7°$) the cross peak vanishes in the $\langle zxzx\rangle$ signal while the $\langle zzzz\rangle$ cross peak contribution is reduced by a factor of 5/9 from its strength in the parallel case. The value of P_2 is negative when the transition dipole angle is between θ_m and $\pi - \theta_m$. The negative angular factor causes a sign change in the cross peak spectral signal along the ω_t-axis. On the other hand, for the $\langle zzzz\rangle$ tensor the angular pre-factor is positive for all choices of the angle between the dipoles. To seek information about the angles between the amide transition dipoles, the 2D IR spectra were recorded in three polarizations corresponding to the tensor components $\langle zzzz\rangle$, $\langle zxxz\rangle$, and $\langle zxzx\rangle$. The signals in Figure 7 were obtained from the 2D IR spectra of the isotopomer II (Figure 5c) by the procedure $\sum_{\omega_\tau}[\underline{S}_R(-\omega_\tau,0,\omega_t) + \underline{S}_{NR}(\omega_\tau,0,\omega_t)]$ $G(\omega_\tau - \omega_0, \sigma)$, where the sum is over the discrete values of ω_τ in the whole spectral region for a given set of polarization conditions, and ω_0 was set to either 1632 cm^{-1} (a, b) or 1602 cm^{-1} (c, d). The function $G(\omega_\tau - \omega_0, \sigma)$is a Gaussian centered at ω_0 having standard deviation σ (3 cm^{-1}). Although our anisotropy experiments could not pinpoint a pair of (ϕ, ψ) angles for isotopomer I, because of the very small off-diagonal anharmonicity of the alanine dipeptide in water, we observed distinctive differences between the two spectra of $\underline{S}_{zzzz}(\omega_\tau,T = 0,\omega_t)$ and $3\underline{S}_{zxxz}(\omega_\tau,T = 0,\omega_t)$ in the cross peak regions for the isotopomer II. The magnitude of $\underline{S}_{zzzz}(1632, 0, 1602) - 3\underline{S}_{zxxz}$-(1632,0,1602) at the cross peak regions was about 4 % of that at the diagonal region, $\underline{S}_{zzzz}(1602,0,1602)$, as shown in Figure 7a, b. We attribute these results to the existence of an off-diagonal anharmonicity between the two amide-I′ modes. If it is assumed that the cross peaks are due the coupling between the modes, an estimate consistent with all our spectra yielded an apparent off-diagonal anharmonicity of $\Delta_{12} = 0.2 \pm 0.2$cm^{-1}, which corresponds to an apparent coupling between the amide units of $|\beta| = 1.5 \pm 0.5$ cm^{-1} using a perturbation formula[34] for the off-diagonal anharmonicity in terms of the coupling and the diagonal anharmonicity $\Delta{:}\Delta_{12} = 4\beta^2\Delta/((\omega_2 - \omega_1)^2 - \Delta^2)$. This measurement defines the maximum contribution of the coupling to the cross peak region; as discussed below the very weak cross peaks could occur at zero coupling for certain choices of the dynamical parameters. The tail of diagonal peak at the cross peak region was 1/3 of that of $\underline{S}_{zzzz}(1602,0,1602)$. The existence of the diagonal spectrum at the cross peak region makes it impossible to obtain a reliable ratio of cross peak intensities for the two polarizations, $\langle zzzz\rangle_{cross}/3\langle zxxz\rangle_{cross}$, where $\langle zzzz\rangle_{cross}$ and $\langle zxxz\rangle_{cross}$ represent 2D spectra solely contributed by cross terms of $\langle zzzz\rangle$ and $\langle zxxz\rangle$ polarization, respectively. However, we could place meaningful limits on this ratio that put it in the range of from negative infinity to -2 or from $+4$ to positive infinity. For the case of weak coupling, $\langle zzzz\rangle_{cross}/3\langle zxxz\rangle_{cross} = (4P_2+5)/(9P_2)$ locates an angle $\theta = 52° \pm 10°$ or $\pi-(52° \pm 10°)$. The angle θ is close to the magic angle θ_m. The small coupling suggests θ is unlikely to be near 52°, as discussed later in the paper. So from now on we assume it is $128° \pm 10°$. By varying the coupling from -1.5 to $+1.5$ cm^{-1} and by assuming that the amide-I′ transition dipole makes an angle of 20° to the C═O bond axis,[22] the experimentally determined θ yields a range of Ramachandran angles (ϕ, ψ)= ($-70° \pm 25°$, $+120° \pm 25°$) for the alanine dipeptide. This conformation lies in the neighborhood of the PP_{II} structure which has typical dihedral angles as ($-75°$, $+145°$). Further, the range of ψ also accommodates the C_7 conformation ($-80°$, $+80°$) but with lower probability. On the other hand, a C_5 structure which has typical dihedral angles as ($-150°$, $+150°$) is not likely because the dihedral angle ϕ is too different. The predicted transition dipole coupling of the C_5 conformation is also quite small (~ -2 cm^{-1}). Further, the possibility of the dipeptide having an α_R-like structure can be ruled out because the angle ψ is too different from a typical helical conformation (ca. $-47°$), and also because the nearest neighbor amide-I′ mode coupling at helical conformations is larger than observed: for example, a value of ca. $+7.5$ cm^{-1} was found in an ideal helical conformation ($-58°$, $-47°$) by a DFT calculation[25] and by our recent 2D IR measurement,[18] neither of which correspond to what is observed for the alanine dipeptide.

Simulation of the Linear-IR Spectrum. A recent NMR study,[7] one DFT calculation on the dialanine-water cluster,[3] and two recent all-atom simulations with explicit water molecules,[2,35] suggested a P_{II} conformation as the major component of the alanine dipeptide distribution in the aqueous phase. To further quantify the analysis of the linear-IR spectrum and prepare for the treatment of the 2D IR spectrum we have carried out quantum chemical computations on dialanine at a variety of conformations that exhibit very small coupling in the range indicated by the FTIR and 2D IR spectra. These calculations were performed on dipeptides in vacuo, not in water, so

TABLE 1: Calculated Amide-I′ Normal Mode Transition Frequencies ν_k (cm^{-1}), Intensity I_k (km/mol), Dipole Moment Magnitude $|\mu_k|$ (Debye), and Potential Energy Distributions (PED) of the Amide Unit (O═C−ND) and C═O Group Only of the Alanine Dipeptide (N−D) Isotopomers[a]

				$PED_{amide\ unit}$		$PED_{C=O}$	
[Ac-end, Am-end]	ν_k	I_k	$\|\mu_k\|$	Ac-end	Am-end	Ac-end	Am-end
[^{12}C═^{16}O, ^{12}C═^{16}O]	1640.4 (1749.2)	251.2	0.239	0.0	72.6	0.0	69.6
	1632.6 (1740.9)	273.8	0.250	83.3	0.0	80.0	0.0
I, [^{13}C═^{16}O, ^{12}C═^{16}O]	1640.4 (1749.2)	251.2	0.239	0.0	72.6	0.0	69.6
	1591.2 (1696.7)	258.6	0.247	80.3	0.0	76.8	0.0
II, [^{12}C═^{16}O, ^{13}C═^{16}O]	1632.5 (1740.8)	273.3	0.250	83.3	0.0	80.0	0.0
	1598.9 (1705.0)	236.1	0.235	0.0	66.7	0.0	63.8

[a] The backbone dihedral angles are (−75°, +135°) and the coupling between two modes is $\beta = -0.1$ cm^{-1}. A frequency scaling factor was determined to be 0.9378, chosen to fit the FTIR measurements of three isotopomers. The calculated frequency, without scaling, is listed in the parentheses.

conclusions drawn from them assume the nearest neighbor coupling in the dipeptide is dependent on the peptide geometry but not directly on the interactions with solvent. Furthermore, in this work the structures are chosen without regard to their stabilization energy in the gas phase, our goal being to evaluate coupling constants. A simple calculation of the transition dipole coupling between amide-I′ modes of dialanine as a function of ϕ and ψ dihedral angles showed several narrow regions in which the coupling is in the range of 1 cm^{-1} or less.[5] One such domain lies between the C_5 and C_{7eq} structures. A total of 24 conformations were initially constructed in this domain, by varying the backbone dihedral angles in a step of 5° in a subspace ($-85° \le \phi \le -75°$, $+115° \le \psi \le +150°$), that encompasses ideal PP_{II} conformation (−75°, +145°).

The ab initio DFT calculations at the B3LYP/6-31+G* level were carried out by using the Gaussian03 package.[36] The dipeptides were treated in their deuterated form (ND) in vacuo. Default convergence in Gaussian03 was used during geometry optimization of each conformation. Normal-mode analysis was performed on the energy minimized structure. Two amide-I′ local mode frequencies and the total vibrational coupling (β) between them were obtained by decomposing the calculated normal modes into local amide-I′ modes on the acetyl and amino ends of the peptide, as described previously.[25] It was found that in most cases the two local mode frequencies are different, consistent with their different chemical environments. The smallest values of the coupling, $|\beta| \le 0.5$ cm^{-1}, were found in the dihedral angle ranging from ($\phi = -85°$, $\psi = +125° \sim +135°$) to ($\phi = -75°$, $\psi = +130° \sim +138°$). One conformation, which we refer to as "L" having angles as (−75°, +135°), was found to have the weakest coupling (−0.01 cm^{-1}) of all, consequently two amide-I′ normal modes are essentially localized. The amide-I′ local mode properties, including the transition frequencies, intensities, transition dipole moments, and the potential energy distribution (PED)[37] for three isotopomers in the L conformation are listed in Table 1. The mode frequencies were scaled by a factor 0.9378, by fitting the six calculated transition frequencies to the experimental data. This factor is typical for such computations[38] and is known to depend on the basis set and on the molecular sets used in the computation as well. The scaled transition frequencies, for example for the isotopomer I, are 1591.2 and 1640.4 cm^{-1} and are within ±2.6 cm^{-1} of the measured values. The scaled zero-order isotopic shift is ca. 41.1 cm^{-1}, in excellent agreement with measurement (40 − 41.5 cm^{-1}). The transition dipole coupling for L was estimated to be −1.48 cm^{-1}, indicating that it is not a good approximation to the coupling for this configuration. The through-bond interaction is almost as strong as the through-space contribution in L but opposite sign so that the two contributions cancel out. The PED results show that in the unsubstituted form, the overall contributions of atomic displacements of the acetyl end amide unit (C, O, N, and D) to the 1632.6 cm^{-1} transition is greater than 83% (with 80% of this coming from C═O only), whereas the contribution of the amino end amide unit to this mode is negligible. This is consistent with the fact that the DFT coupling is nearly zero and the mode is highly localized on the amide unit at the acetyl end. A similar situation was found for the 1640.4 cm^{-1} in which the amino end amide unit dominates (72.6%). The difference in the PED values in these two modes is consistent with the difference in their transition intensities. Upon ^{13}C-substitution, the dominant PED value drops by ca. 3% (for the acetyl end) and ca. 6% (for the amino end). These changes suggest that an increased degree of mixing occurs between the amide-I′ and other modes in ^{13}C− than in ^{12}C-isotopomers. Normal mode calculations also suggest there is ca. 3−4% decrease in the frequency-corrected transition dipole magnitude in ^{13}C− than in ^{12}C-isotopomers, in agreement with the PED analysis. These calculations are in agreement with the experiments that the small intensity differences between the acetyl and amino end amide-I′ groups are not caused by coupling between them. In addition, our DFT calculation shows that the angle between the amide-I′ transition dipole and the corresponding C═O bond axis in two amide units are slightly different in peptide oligomers; it is 14° for the acetyl end and 22° for the amino end in the L conformation. This leads to an angle of 142° between two transition dipoles. This theoretical result is in agreement with the assumption that the angle between the dipole and the amide C═O bond axis may vary from 10° to 25° in peptide oligomers.[22,39] When this angle is set to 20° for both amide units for L the angle between two dipoles is 137°.

The calculated IR spectra of three isotopomers are shown in Figure 8 where Voigt profiles, incorporating a homogeneous width parameter, γ_{01}, and in inhomogeneous parameter, σ_{01}, were employed. For the unlabeled peptide, $\gamma_{01} = 8.7$ and 10.4 cm^{-1} and $\sigma_{01} = 8.5$ and 9.2 cm^{-1} were used for the amino and acetyl ends, respectively. For the isotopomer I, the values are $\gamma_{01} = 8.2$ and 10.4 cm^{-1} and $\sigma_{01} = 8.5$ and 9.6 cm^{-1}; for isotopomer II, they are $\gamma_{01} = 6.9$ and 10.4 cm^{-1} and $\sigma_{01} = 7.6$ and 9.5 cm^{-1}. These parameters were derived based on FTIR, pump−probe, and 2D IR measurements. The calculated normal mode transition frequency was consistent with experiment inasmuch as the low frequency was attributed to the amide unit at the acetyl end of the unsubstituted compound and the isotopomer I, whereas for isotopomer II the amino end had the lowest frequency. However, the underlying transition dipole strengths in each case were somewhat different from the experiment, as outlined in Table 1. For example, the intensity ratio of the acetyl to amino was found to be 1: 0.97 for the isotopomer I from calculation, whereas it was 0.905:1 from

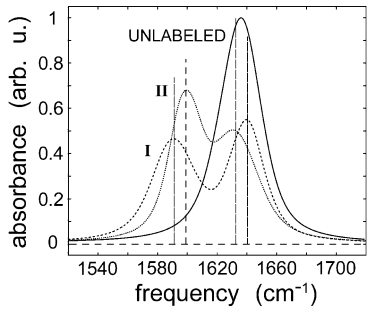

Figure 8. Calculated linear IR spectra of alanine dipeptide isotopomers in the ND form based on ab initio DFT results. Three curves are labeled in the same way as Figure 1. The dihedral angles were chosen to be (−75°, +135°). Voigt profiles were used for each transition. The vertical lines indicate roughly the central frequencies of each band.

FTIR measurement. In addition, it was found none of the 24 conformations generated the experimental values of the ratio of integrated areas for all three isotopomers. It is generally known that the transition frequencies predicted using DFT calculations are in reasonable agreement with experiments upon scaling,[40−43] but the predicted transition intensities are often less accurate.

The DFT calculations in the neighborhood of the PP_{II}-like conformations yield parameters consistent with experiments. We explored other regions in the conformation space where the calculated transition dipole coupling is expected to be weak: namely, at the lower left region near (−75°, −135°), the upper right region near (+75°, +135°), and the lower right region near (+75°, −135°). The first two choices correspond to θ near 52°. Four points were randomly chosen within each of these (ϕ, ψ) domains. None of the normal mode frequency patterns in these regions fitted the experimental data. The acetyl end amide was predicted to have a higher amide-I′ frequency in all these three regions, which is inconsistent with linear-IR results. Further, the total coupling from DFT in the lower left and upper right regions is larger than +9.0 cm^{-1}, strongly suggesting that these conformations are not being seen in the 2D IR results, and that the angle between two transition dipole moments is not in the vicinity of θ but rather $\pi-\theta$. In addition, DFT calculations show that a 3_{10}-like conformation (−50°, −25°) has a small coupling, however, the angle between transition dipoles in this case is not consistent with the polarized IR experiments.

Simulations of the 2D IR Spectra. The response functions that have often been used to describe the cross peaks in 2D IR spectra have the property that they do not go to zero smoothly as the coupling between the modes goes to zero.[24,34] However, it is apparent that when modes are completely uncoupled, the nonlinear response of one local mode cannot depend on whether other modes are excited. Therefore, in that event there should be no cross peak in the 2D IR signal. Furthermore, it is well-known that the cross peak signal is sensitive to the correlations of the frequency fluctuations in the two distributions. With such weakly coupled modes it is unlikely that there is any measurable correlation between their fluctuations. Therefore, in what follows we will first assume that they are uncorrelated.

The experimental results for the waiting time dependence of the 2D IR spectra have shown that the appearance of the 2D IR spectra are not very sensitive to the spectral diffusion.[34] In addition it has been shown that there is a significant inhomogeneous distribution that is fixed over the time scales dominating the present experiments. Therefore, we have used Bloch dynamics in 2D IR simulation presented here. The scaled transition frequencies and unscaled transition dipole moments μ_1^2 and μ_2^2 were taken from the DFT results for three isotopomers along with the dynamical parameters discussed above. The 2D IR spectrum was computed from the formula:[25,32]

$$S(\mp\omega_\tau,\omega_t) = \left\langle \sum_{k,k'} \frac{\langle 4P_2(\cos\theta_{kk'}) + 5\rangle \mu_k^2 \mu_{k'}^2}{[-i(\mp\omega_{k0} - \omega_\tau) - \gamma_{k0}]} \times \left\{ \frac{1}{[i(\omega_{k'0} - \omega_t) + \gamma_{k'0}]} - \sum_K \frac{1}{[i(\omega_{Kk} - \omega_t) + \gamma_{Kk}]} \right\} \right\rangle \quad (4)$$

where the "−" and "+" in "∓" on both sides of the equation designate the rephasing and the non-rephasing parts of the signal, respectively. The indices k, k' run over the singly excited state $|1\rangle$ and $|2\rangle$ corresponding to the amino and acetyl ends, while K runs over the doubly excited states $|1+1\rangle$, $|1+2\rangle$ and $|2+2\rangle$. The outer average is over the uncorrelated inhomogeneous distributions of the two oscillators and the inner ones are over an isotropic angular distribution with z being a laboratory fixed polarization vector. As described previously the frequencies were calculated by diagonalization of the 5 × 5 matrix of one and two particle excitations for the dipeptide amide-I′ modes using the couplings and coordinates from the calculation. The inhomogeneity was introduced by adding the results of 10,000 such diagonalizations with diagonal elements chosen from a Gaussian distribution characterized by the appropriate σ. The $k \rightarrow k + k$ squared transition dipoles are chosen to be twice those for $0 \rightarrow k$: the experimental pump−probe spectral intensities justify this condition.

The L conformation at the dihedral angle (−75°, +135°) is chosen as the typical situation in which the coupling is negligible and is consistent with linear-IR simulation in Figure 8. A set of values for the total dephasing of the υ=1 → υ=2 transitions were $\gamma_{1,1+1}$ = 13.3 and $\gamma_{2,2+2}$=16.8 cm^{-1} (the isotopomer I) and $\gamma_{1,1+1}$ = 11.5 and $\gamma_{2,2+2}$ = 16.8 cm^{-1} (the isotopomer II) for amides at the amino and acetyl ends, respectively. These parameters assume that the population relaxation time is the same for the υ=1 and υ=2 states. When this condition is made more conventional and the υ=2 relaxations are chosen to be twice as fast as those of υ=1, these values became even larger. Simulations using these parameters result in much broadened line width of the $\upsilon = 1 \rightarrow \upsilon = 2$ transitions for both vibrators in both isotopomers. This is not in agreement with the results shown in Figures 4, 5 and 7; in Figure 7 slices cut through the ω_τ-axis indicate that the total width of the υ=1 → υ=2 transition is no more than 1.2 times of that of the υ=0 → υ=1 transition. This suggests that $\gamma_{k,k+k} \approx 1.2 \cdot \gamma_{0k}$ (for k=1,2) should be set for two vibrators in the 2D IR simulation. It is not uncommon that the $\upsilon = 1 \rightarrow \upsilon = 2$ and $\upsilon = 0 \rightarrow \upsilon = 1$ transitions may have a similar width, for example, as seen in a pump−probe spectrum. The discrepancy between parameters derived from FTIR and pump−probe and those observed from the 2D IR spectra could mean that the dephasing process of $\upsilon = 1 \rightarrow \upsilon = 2$ requires a different frequency fluctuation correlation function.

Figure 9 shows the simulated real part of the correlation 2D IR spectra for the isotopomers I and II at zero waiting time (T = 0). Two cases are compared by incorporating either zero coupling (a, b) or a small coupling, β = +1.5 cm^{-1} (c, d). The simulation reproduces most of the essential features of experimental results of this two-vibrator system at T = 0 shown in Figure 5, including the profile of the diagonal peaks (absolute peak positions and relative peak intensities), and the weak off-

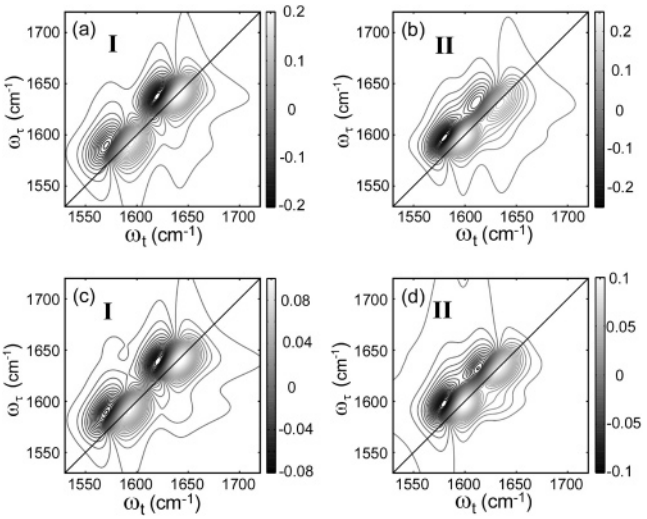

Figure 9. Calculated absorptive 2D IR spectra of the alanine dipeptide isotopomers I and II at zero waiting time ($T = 0$), based on ab initio DFT results. Only the real parts are shown. (a, c) are the isotopomer I; (b, d) are the isotopomer II. The coupling β was set to zero in (a, b) and to $+1.5$ cm^{-1} in (c, d).

diagonal cross peaks. It is observed that the cross peak is more evident when two vibrators are closer (the isotopomer II), an observation in agreement with experiment (the correlation spectra shown in Figure 5). In the case of zero coupling (a, b), the off-diagonal peaks are not obvious, because of the difference in the total dephasing time for the $v=0 \rightarrow v=1$ and $v=1 \rightarrow v=2$ transitions is chosen to be only 20% for each vibrator. However, they still can be seen more clearly in the simulated rephasing and non-rephasing spectra (data not shown). Further, because these cross peaks are not due to coupling, they have no polarization dependence even though the angle between two transition dipoles is ca. 137°: the profile of 2D IR spectra in the $\langle zzzz \rangle$ polarization for zero coupling is exactly three times of that in the $\langle zxxz \rangle$ polarization. When assuming a positive correlation between two vibrators' $v=0 \rightarrow v=1$ transition frequency fluctuations, the cross peaks are enhanced, and differ in the $\langle zzzz \rangle$ and $\langle zxxz \rangle$ polarizations. When introducing a small coupling ($\beta = +1.5$ cm^{-1}), the 2D IR spectra for these two isotopomers show more pronounced cross peaks (Figure 9c, d). Using the isotopomer II as an example, the difference between $\underline{S}_{zzzz}(1632, 0, 1600)$ and $3\,\underline{S}_{zxxz}(1632, 0, 1600)$ is ca. 2−3% of the diagonal signal at $\underline{S}_{zzzz}(1600, 0, 1600)$, which is in a reasonable agreement with what was estimated from Figure 7. Further increasing the magnitude of the coupling to greater than 3.0 cm^{-1} yields an unreasonably stronger cross peak signal especially for the isotopomer II. The introduction of a positive correlation coefficient into the $v=0 \rightarrow v=1$ transition frequency fluctuations of two vibrators also causes an increase in the cross peak intensity in this case.

The relationship between the off-diagonal anharmonicity Δ_{12} and the coupling β was further examined by simulation. The value of Δ_{12} can be obtained by a Hamiltonian matrix diagonalization of two vibrators representing the amides at the acetyl and amino ends. An exponential-like distribution was obtained from an ensemble of 25 000 calculations assuming two uncorrelated $v=0 \rightarrow v=1$ transition frequencies. The zero order frequencies and the variances of Gaussian distributions used were the same as determined earlier in the paper. It was found that the most probable value of Δ_{12} was 0.06 cm^{-1} for the isotopomer I and 0.08 cm^{-1} for the isotopomer II when the coupling was set to $+1.5$ cm^{-1}. These two values became 0.08 and 0.12 cm^{-1} when the coupling was set to $+2.0$ cm^{-1}. These values were in a reasonable agreement with those derived from the experiment, namely $\Delta_{12} = 0.2 \pm 0.2$ cm^{-1}, leading to $|\beta| = 1.5 \pm 0.5$ cm^{-1}. In addition, an increase of less than 10% in the off-diagonal anharmonicity was observed when the two vibrators are fully correlated in their $v=0 \rightarrow v=1$ transition frequency fluctuations. The apparent off-diagonal anharmonicity is more influenced by the ratio of the inhomogeneous to homogeneous widths than by correlation. These results are again consistent with a small coupling constant in the range observed. The increase by 24 cm^{-1} (see Figure 1b) of the frequency separation between the acetyl and amino end amide-I′ transitions in the isotopomer I compared with II should cause a change in the relative intensities of the upper and lower transition frequencies if there is coupling that causes intensity transfer. A coupling of $+1.5$ cm^{-1} is predicted to change this ratio by ca. 2.5% in a PP_{II} structure, which is consistent with the FTIR spectra.

The correlations between the $v=0 \rightarrow v=1$ transition frequency fluctuations of two amide-I′ modes in the subspace of ($-85° \leq \phi \leq -75°$, $+115° \leq \psi \leq +150°$) were examined by DFT calculation. The normal mode calculation on 24 structures shows that the frequency of the amino end changes from 1746 to 1751 cm^{-1} (unscaled), and that of the acetyl end from 1731 to 1748 cm^{-1}. The overall correlation coefficient for the amino and acetyl end frequency variations in this region is found to be $+0.15$. Thus the two amide-I′ mode frequencies are not well correlated, even for the dipeptide in a vacuum. The solvent fluctuations are likely to reduce the correlation even more, leading to uncorrelated transitions, in agreement with the indications from experiment.

The 2D IR simulation was also carried out using the frequency correlation function determined from experiments.[27] Taking the isotopomer II as an example, it was found that the difference ($\underline{S}_{zzzz} - 3\underline{S}_{zxxz}$) is increased by ca. 20−30% over that obtained using the Bloch model, assuming a similar coupling constant. Therefore, two models give essentially the same cross peak shape and intensity.

Conclusions

Two IR bands in the amide-I′ region have been assigned unambiguously by using ^{13}C isotopic substitutions, showing that the amide unit at the acetyl end has a lower transition frequency in the unlabeled species. Spectral characteristics in both linear-IR and 2D IR indicate that two amide-I′ modes are highly localized. Very small changes in the ratio of the transition dipole strengths of the amides at the acetyl end and amino end were found for two amide-I′ bands in the linear-IR spectra of the dipeptide isotopomers, suggesting no significant intensity transfer between two vibrators and hence a weak intramode coupling. In 2D IR spectra the cross peaks directly associated with coupling were found to be discernible in both isotopomers. The coupling is estimated as $|\beta| = 1.5 \pm 0.5$ cm^{-1}. The diagonal anharmonicities for two vibrators were found to be ca. 15.5 and 16.0 cm^{-1} for the amino end and acetyl end by using one- and two-quantum 2D IR, whereas the off-diagonal anharmonicity was found to be very small ($\Delta_{12} = 0.2 \pm 0.2$ cm^{-1}). The difference in the 2D IR spectra in two polarizations ($\langle zzzz \rangle$ vs $\langle zxxz \rangle$) predicted an angle between the two transition dipoles of $52° \pm 10°$, or $\pi - (52° \pm 10°)$, suggesting most probably a PP_{II}-like conformation with Ramachandran angles ($-70° \pm 25°$, $+120° \pm 25°$). The population relaxation times for the amide-I′ mode of the amino and acetyl end were found to be 576 and 415 fs for the isotopomer I from the transient grating measure-

ments, thereby accounting for ca. 50% of the total dephasing width of the $v=0 \rightarrow v=1$ transitions. Ab initio DFT calculations and normal mode decoupling analysis have been carried out in the Ramachandran subspace near the PP_{II} conformation. The results confirm the weak coupling in the dipeptide at that configuration and support the experimental findings. Simulations of linear-IR and 2D IR incorporating the scaled transition frequencies and transition dipole moments from DFT calculations for the conformation at (−75°, +135°) could reproduce the experimental linear spectra and coupling from 2D IR. The simulation was carried out in the frequency-domain directly assuming Bloch dynamics. The possible range of coupling magnitude and the influence of frequency fluctuation correlations on the cross peaks have been explored. The experimental measurements and supportive simulations are consistent with a PP_{II}-like conformation for the alanine dipeptide in aqueous solution, in which two amide-I′ modes are highly localized and their frequency fluctuations are uncorrelated with one another.

Acknowledgment. This research was supported by grants from NIH (GM12592 and RR01348) and NSF to R.M.H.

References and Notes

(1) Madison, V.; Kopple, K. D. *J. Am. Chem. Soc.* **1980**, *102*, 4855.
(2) Drozdov, A. N.; Grossfield, A.; Pappu, R. V. *J. Am. Chem. Soc.* **2004**, *126*, 2574.
(3) Han, W.-G.; Jalkanen, K. J.; Elstner, M.; Suhai, S. *J. Phys. Chem. B* **1998**, *102*, 2587.
(4) Mehta, M. A.; Fry, E. A.; Eddy, M. T.; Dedeo, M. T.; Anagnost, A. E.; Long, J. R. *J. Phys. Chem. B* **2004**, *108*, 2777.
(5) Gnanakaran, S.; Hochstrasser, R. M. *J. Am. Chem. Soc.* **2001**, *123*, 12886.
(6) Takekiyo, T.; Imai, T.; Kato, M.; Taniguchi, Y. *Biopolymers* **2004**, *73*, 283.
(7) Poon, C.-D.; Samulski, E. T.; Weise, C. F.; Weisshaar, J. C. *J. Am. Chem. Soc.* **2000**, *122*, 5642.
(8) Brooks, B. R.; Bruccoleri, R. E.; Olafson, B. D.; States, D. J.; Swaminathan, S.; Karplus, M. *J. Comput. Chem.* **1983**, *4*, 187.
(9) Hamm, P.; Lim, M.; Hochstrasser, R. M. *J. Phys. Chem. B* **1998**, *102*, 6123.
(10) Asplund, M. C.; Zanni, M. T.; Hochstrasser, R. M. *Proc. Natl. Acad. Sci. U.S.A.* **2000**, *97*, 8219.
(11) Golonzka, O.; Khalil, M.; Demirdoven, N.; Tokmakoff, A. *Phys. Rev. Lett.* **2001**, *86*, 2154.
(12) Zhang, W. M.; Chernyak, V.; Mukamel, S. *J. Chem. Phys.* **1999**, *110*, 5011.
(13) Hamm, P.; Lim, M.; DeGrado, W. F.; Hochstrasser, R. M. *Proc. Natl. Acad. Sci. U.S.A.* **1999**, *96*, 2036.
(14) Zanni, M. T.; Gnanakaran, S.; Stenger, J.; Hochstrasser, R. M. *J. Phys. Chem. B* **2001**, *105*, 6520.
(15) Rubtsov, I. V.; Wang, J.; Hochstrasser, R. M. *J. Phys. Chem. A* **2003**, *107*, 3384.
(16) Rubtsov, I. V.; Wang, J.; Hochstrasser Robin, M. *Proc. Natl. Acad. Sci. U.S.A.* **2003**, *100*, 5601.
(17) Rubtsov, I. V.; Wang, J.-P.; Hochstrasser, R. M. *J. Chem. Phys.* **2003**, *118*, 7733.
(18) Fang, C.; Wang, J.; Kim, Y. S.; Charnley, A. K.; Barber-Armstrong, W.; Smith, A. B., III.; Decatur, S. M.; Hochstrasser, R. M. *J. Phys. Chem. B* **2004**, *108*, 10415.
(19) Fleming, G. R.; Cho, M. *Annu. Rev. Phys. Chem.* **1996**, *47*, 109.
(20) Dorrer, C.; Belabas, N.; Likforman, J.-P.; Joffre, M. *J. Opt. Soc. Am. B: Opt. Phys.* **2000**, *17*, 1795.
(21) Lepetit, L.; Cheriaux, G.; Joffre, M. *J. Opt. Soc. Am. B: Opt. Phys.* **1995**, *12*, 2467.
(22) Torii, H.; Tasumi, M. *J. Chem. Phys.* **1992**, *96*, 3379.
(23) Lim, M.; Hochstrasser, R. M. *J. Chem. Phys.* **2001**, *115*, 7629.
(24) Ge, N.-H.; Zanni, M. T.; Hochstrasser, R. M. *J. Phys. Chem. A* **2002**, *106*, 962.
(25) Wang, J.; Hochstrasser, R. M. *Chem. Phys.* **2004**, *297*, 195.
(26) Mukamel, S. *Principles of Nonlinear Optical Spectrscopy*; Oxford University Press: Oxford, 1995.
(27) Kim, Y. S.; Hochstrasser, R. M. *J. Phys. Chem. B*, in press.
(28) Ernst, R. R. *Principles of Nuclear Magnetic Resonances in One and Two Dimensions*; Oxford Univerity Press: Oxford, 1987.
(29) Khalil, M.; Demirdoven, N.; Tokmakoff, A. *Phys. Rev. Lett.* **2003**, *90*, 047401/1.
(30) Ge, N.-H.; Hochstrasser, R. M. *PhysChemComm* **2002**, Paper No 3.
(31) Fulmer, E. C.; Mukherjee, P.; Krummel, A. T.; Zanni, M. T. *J. Chem. Phys.* **2004**, *120*, 8067.
(32) Hochstrasser, R. M. *Chem. Phys.* **2001**, *266*, 273.
(33) Zanni, M. T.; Ge, N.-H.; Kim, Y. S.; Hochstrasser, R. M. *Proc. Natl. Acad. Sci. U.S.A.* **2001**, *98*, 11265.
(34) Hamm, P.; Hochstrasser, R. M. Structure and dynamics of proteins and peptides: femtosecond two-dimensional infrared spectroscopy. In *Ultrafast Infrared and Raman Spectroscopy*; Fayer, M. D., Ed.; Marcel Dekker Inc.: New York, 2001; p 273.
(35) Gnanakaran, S.; Garcia, A. E. *J. Phys. Chem. B* **2003**, *107*, 12555.
(36) Frisch, M. J.; Trucks, G. W.; Schlegel, H. B.; Scuseria, G. E.; Robb, M. A.; Cheeseman, J. R.; Montgomery, J. A., Jr.; Vreven, T.; Kudin, K. N.; Burant, J. C.; Millam, J. M.; Iyengar, S. S.; Tomasi, J.; Barone, V.; Mennucci, B.; Cossi, M.; Scalmani, G.; Rega, N.; Petersson, G. A.; Nakatsuji, H.; Hada, M.; Ehara, M.; Toyota, K.; Fukuda, R.; Hasegawa, J.; Ishida, M.; Nakajima, T.; Honda, Y.; Kitao, O.; Nakai, H.; Klene, M.; Li, X.; Knox, J. E.; Hratchian, H. P.; Cross, J. B.; Adamo, C.; Jaramillo, J.; Gomperts, R.; Stratmann, R. E.; Yazyev, O.; Austin, A. J.; Cammi, R.; Pomelli, C.; Ochterski, J. W.; Ayala, P. Y.; Morokuma, K.; Voth, G. A.; Salvador, P.; Dannenberg, J. J.; Zakrzewski, V. G.; Dapprich, S.; Daniels, A. D.; Strain, M. C.; Farkas, O.; Malick, D. K.; Rabuck, A. D.; Raghavachari, K.; Foresman, J. B.; Ortiz, J. V.; Cui, Q.; Baboul, A. G.; Clifford, S.; Cioslowski, J.; Stefanov, B. B.; Liu, G.; Liashenko, A.; Piskorz, P.; Komaromi, I.; Martin, R. L.; Fox, D. J.; Keith, T.; Al-Laham, M. A.; Peng, C. Y.; Nanayakkara, A.; Challacombe, M.; Gill, P. M. W.; Johnson, B.; Chen, W.; Wong, M. W.; Gonzalez, C.; Pople, J. A. *Gaussian 03*, revision B.01; Gaussian, Inc.: Pittsburgh, PA, 2003.
(37) Califano, S. *Vibrational states*; John Wiley and Sons: New York, 1976.
(38) Foresman, J. B.; Frisch, A. *Exploring chemistry with electronic structure methods*; Gaussian Inc.: Pittsburgh, 1996.
(39) Torii, H.; Tasumi, M. *J. Raman Spectrosc.* **1998**, *29*, 81.
(40) Matsuura, H.; Yoshida, H. Calculation of vibrational frequencies by Hartree-Fork-based and density function theory. In *Handbook of Vibrational Spectroscopy*; Chalmers, J. M., Griffiths, P. R., Eds.; John Wiley & Sons: Chichester, 2002; Vol. 3, pp 2012−2028.
(41) Johnson, B. G.; Gill, P. M. W.; Pople, J. A. *J. Chem. Phys.* **1993**, *98*, 5612.
(42) Rauhut, G.; Pulay, P. *J. Phys. Chem.* **1995**, *99*, 3093.
(43) Scott, A. P.; Radom, L. *J. Phys. Chem.* **1996**, *100*, 16502.